

### Supporting Information

## Visualization of Domain Structure and Piezoelectric Energy Harvesting in a Ferroelectric Metal-Ligand Cage

Neetu Prajesh,<sup>a</sup> Dipti R. Naphade,<sup>†,b</sup> Ashok Yadav,<sup>†,a</sup> Vikash Kushwaha,<sup>a</sup> Balu Praveenkumar,<sup>\*,c</sup> Jan K. Zaręba,<sup>\*,d</sup> Thomas D. Anthopoulos,<sup>\*,b</sup> Ramamoorthy Boomishankar<sup>\*,a</sup>

<sup>a</sup>Department of Chemistry and <sup>†</sup>Centre for Energy Science, Indian Institute of Science Education and Research (IISER), Pune, Dr. Homi Bhabha Road, Pune – 411008, India

*E-mail:* [boomi@iiserpune.ac.in](mailto:boomi@iiserpune.ac.in)

<sup>b</sup>King Abdullah University of Science and Technology (KAUST), KAUST Solar Center (KSC) Thuwal 23955-6900 (Saudi Arabia). *E-mail:* [Thomas.anthopoulos@kaust.edu.sa](mailto:Thomas.anthopoulos@kaust.edu.sa)

<sup>c</sup>PZT Centre, Armament Research and Development Establishment (ARDE), Dr. Homi Bhabha Road, Pune – 411008, India

*E-mail:* [praveenkumar@arde.drdo.in](mailto:praveenkumar@arde.drdo.in)

<sup>d</sup>Institute of Advanced Materials, Wrocław University of Science and Technology, 50-370, Wrocław, Poland

*E-mail:* [jan.zareba@pwr.edu.pl](mailto:jan.zareba@pwr.edu.pl)

## Table of Contents

| S.No | Contents  | Page No. |
|------|---|----------|
| 1.   | Experimental Procedures                                       | S3-S4    |
| 2.   | X-ray Crystallographic Information                            | S5       |
| 3.   | Characterization Data for <b>1</b>                            | S6-S7    |
| 4.   | SHG data  | S8       |
| 5.   | Material Characterization of <b>1</b>                         | S8-S13   |
| 6.   | PFM data of <b>1</b>  | S13-S14  |
| 6.   | Characterization and testing of <b>1</b> -TPU composite films | S14-S20  |
| 7.   | References  | S20-S21  |

## EXPERIMENTAL SECTION

**General Remarks.** All manipulations involving phosphorous halides and solvent purification were performed under a dry nitrogen atmosphere in standard Schlenk-glassware. The precursors  $\text{Ni}(\text{NO}_3)_2 \cdot 6\text{H}_2\text{O}$  and 3-aminopyridine was purchased from Merck and used as received.  $\text{PSCl}_3$  was purchased locally and was distilled prior to use. The ligand **TPTA** was synthesized by following our earlier reported procedure.<sup>1</sup> The powder X-ray diffraction (PXRD) data were obtained from a Bruker-D8 Advance diffractometer. Thermal analysis (TGA) data have been obtained from a Perkin-Elmer STA-6000 thermogravimetric analyzer. Elemental analyses were performed on a Vario-EL cube elemental analyzer. FT-IR in attenuated total reflectance (ATR) mode was taken on neat samples on a Bruker Alpha spectrophotometer. Melting point were obtained using an Electro thermal melting point apparatus and were uncorrected.

**Compound 1:** To a stirred solution of **TPTA** (40 mg, 0.116 mmol) in MeOH (4 mL),  $\text{Ni}(\text{NO}_3)_2 \cdot 6\text{H}_2\text{O}$  (102 mg, 0.350 mmol) in  $\text{H}_2\text{O}$  (1 mL) was added dropwise. The resulting blue solution was filtered through a cellite pad and left for crystallization. The suitable blue block crystals for SCXRD analysis were obtained after five days. Yield: 62 %. M.P. 190-195 °C. FT-IR data on powder ( $\text{cm}^{-1}$ ): 535.75, 693.60, 942.20, 1117.05, 1195.83, 1324.91, 1387.76, 1502.48, 1584.56, 1627.16, 2966.77, 3189.22. Anal. Calcd. for  $\text{C}_{120}\text{H}_{218}\text{N}_{60}\text{O}_{85}\text{P}_8\text{S}_8\text{Ni}_6$ : C, 30.55; H, 4.66; N, 17.81; S, 5.44. Found: C, 30.82; H, 4.94; N, 17.62; S, 5.35.

**Crystallography:** Reflections of **1** were collected on a Bruker Smart Apex Duo diffractometer at 100 K using  $\text{MoK}\alpha$  radiation ( $\lambda = 0.71073 \text{ \AA}$ ). Structures were refined by full-matrix least squares against  $F^2$  using all data using SHELX.<sup>2</sup> All non-hydrogen atoms were refined anisotropically if not stated otherwise. Hydrogen atoms of water molecules were therefore omitted in the refinement due to the high ambiguity in their positions. The nitrate anions and solvates were disordered in the asymmetric unit. The disordered fragments were refined by using similar distances and similar U-restraints (SAME/SIMU) routines of the SHELXL. It is to be noted that the modelling of the anions and the solvent sphere is not ideal due to the diffuse nature of the crystal as seen from the residual electron density map and the fractal coordinates shown in Figure S4.<sup>3</sup>

**Non-linear Optical measurements:** Non-linear optical studies were performed using an attenuated output from a Coherent Astrella Ti:sapphire regenerative amplifier providing 800 nm laser pulses at a 1 kHz repetition rate and of 75 fs duration. A Kurtz-Perry test<sup>4</sup> was performed at 293 K. Potassium dihydrogen phosphate (KDP) was used as a second harmonic generation (SHG) reference. The single crystals of **1** and those of KDP were crushed with a spatula and sieved through a mini-sieve set (Aldrich), collecting a microcrystal size fraction of 250–177  $\mu\text{m}$ . Next, size-graded samples were fixed between microscope glass slides (forming tightly packed layers), sealed, and mounted to the sample holder. Average power of an 800 nm beam, equal to 245 mW, - with a spot area of 0.5  $\text{cm}^2$  was employed. The laser beam was directed onto samples at 45° and was unfocused in all cases. Signal-collecting optics, mounted to the glass optical fiber, were placed perpendicularly to the plane of the sample (backscattering geometry), which was placed on a horizontally aligned holder. Scattered pumping radiation was suppressed using a 750 nm short-pass dielectric filter (FESH0750, Thorlabs). The emission spectra were recorded by an Ocean Optics Flame T spectrograph.

**Preparation of the thin film crystallites of 1 for PFM measurements:** The compound **1** (10 mg) was taken along with 0.5 mL of distilled water in an Eppendorf and sonicated until the dissolution of **1**. The solution was subsequently drop-casted on the Pt substrate and left to stand at room temperature. The blue-coloured micrometer-sized crystallites of **1** were observed on the Pt substrate after one hour.

**Piezoresponse Force Microscopy Characterization:** PFM visualization of the ferroelectric domain structure on **1** microcrystal surface and the thin film was carried out using a commercial AFM system [MFP-3D, Asylum Research in the contact mode (Vector mode)]. A conductive Pt-coated silicon probe was used for domain imaging in lateral and vertical orientation [SCM-PIT-V2 by Bruker, (Pt/Ir coated tip) with a spring constant of 2.8 N/m and a tip radius of 25 nm]. Resonance-enhanced PFM mode was used to enhance the signal with a frequency of 285 kHz and an AC amplitude of 2 V. The  $d_{33}$  values were calculated by recording amplitude the signal at the first contact resonance of the cantilever by changing the tip bias voltage. For non-centrosymmetric materials, due to the converse piezoelectric effect, the Amp (cantilever) =  $d_{33} \times V_{\text{AC}} \times Q_{\text{factor}}$  (tip).<sup>5</sup> We obtained

the amplitude signal by varying the AC bias, and later calculated the  $d_{33}$  values using the above equation. The switching ability of the domains on thin films was checked by the application of external DC bias of  $\pm 50$  V using the PFM tip in contact mode.

**Bulk  $d_{33}$  measurements:** The quasi-static method (known as Berlincourt method) was employed to measure bulk piezoelectric coefficient ( $d_{33}$ ) on the single-crystal of **1**. The force of 0.25 N was used at the tapping frequency of 110 Hz.

**Ferroelectric and Dielectric measurements:** The ferroelectric hysteresis loops for **1** were measured on single crystals of dimensions of 2.33 mm and 2.72 mm by using a Sawyer-Tower circuit. The single crystals were electroded by sticking the aluminium tape on the broad facets of the crystal. The measurements pertaining to the polarization were recorded using a hysteresis loop analyser (TF Analyser 2000E, aixACCT Germany). Leakage current was measured dynamically for various voltage steps during the hysteresis loop measurements.

The dielectric measurements were performed on a powder-pressed sample of **1** compacted in the form of discs (of approximately 10 mm diameter and 1 mm thickness). The compacted discs were subsequently electroded using aluminium adhesive foils for the measurements. The dielectric characteristics of **1** were measured using the Novocontrol, Dielectric Spectrometer.

**Preparation of the 1-PDMS composite films and Testing of the composite devices:** Firstly, the PDMS solution was prepared by adding the silicone elastomer base (Sylgard 184A) and silicone elastomer curing agent (Sylgard 184B) in a 10:1 ratio as stated in the Dow Sylgard 184 Kit. Pre-calculated amounts of **1** were then dispersed into the PDMS to prepare composites of varying (1, 5, 10, 15) weight percent (wt %) compositions. After uniform mixing, the formulated composites were drop-casted onto the aluminium integrated PET sheet with area of 2.5 x 2.5 cm<sup>2</sup> and let it dry for 24 hours followed by placing the aluminium tape of size 2 x 2 cm<sup>2</sup> on the cured composite film. The aluminium integrated PET sheet serves as a bottom electrode and aluminium tape serves as a top electrode. The final device architecture was achieved by establishing electrical contacts to the end of the electrodes followed by the enclosure of the entire device with the Kapton tape to protect the device from any physical damages. Further, the energy harvesting performance of all the **1**-PDMS composite devices was measured by using a home-built impact measurement setup. The output voltages were measured using a Tektronix 2024 mixed-signal oscilloscope operating at an input impedance of 1 M $\Omega$ .

## 2. X-ray Crystallographic Information

Table S1. Crystallographic data for 1.

| Compound                                | 1                                      |
|---|--|
| Chemical formula                        | $C_{120}H_{216}N_{60}Ni_6O_{84}P_8S_8$ |
| Formula weight                          | 4700.02                                |
| Temperature                             | 100 K                                  |
| Crystal system                          | Tetragonal                             |
| Space group                             | I4                                     |
| a (Å); $\alpha$ (°)                     | 21.034(8) Å, 90°                       |
| b (Å); $\beta$ (°)                      | 21.034(8) Å, 90°                       |
| c (Å); $\gamma$ (°)                     | 24.440(9) Å, 90°                       |
| V (Å <sup>3</sup> ); Z                  | 10813(9) Å <sup>3</sup> , 8            |
| $\rho$ (calc.) mg m <sup>-3</sup>       | 1.449                                  |
| $\mu$ (Mo K $\alpha$ ) mm <sup>-1</sup> | 0.747                                  |
| $2\theta_{max}$ (°)                     | 50.484                                 |
| R(int)                                  | 0.0966                                 |
| Completeness to $\theta$                | 100 %                                  |
| Data / param.                           | 9530/606                               |
| GOF                                     | 1.058                                  |
| R1 [F>4 $\sigma$ (F)]                   | 0.1145                                 |
| wR2 (all data)                          | 0.2900                                 |
| max.peak/hole (e.Å <sup>-3</sup> )      | 1.828/-1.214                           |

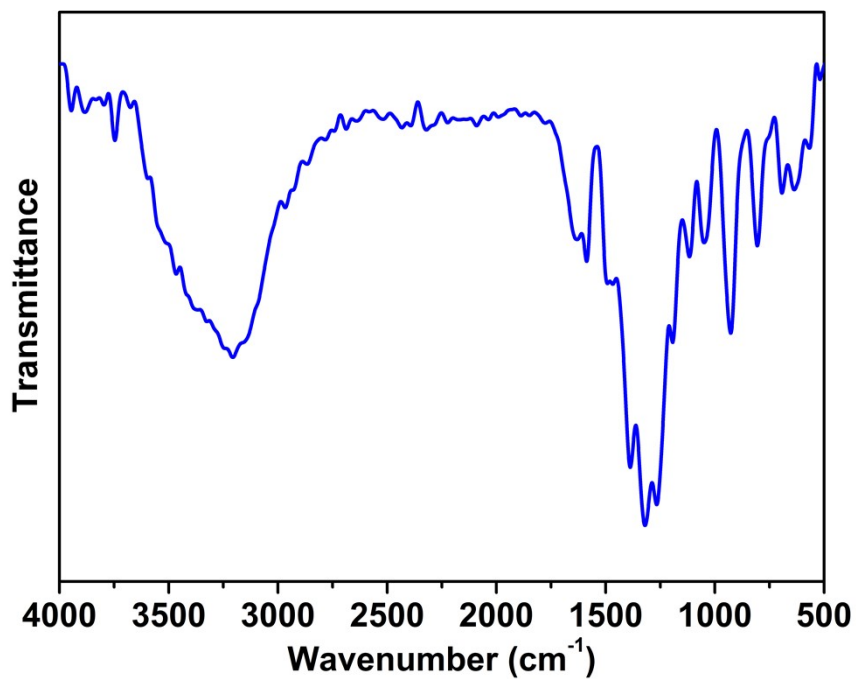


Figure S1 FT-IR spectra of 1.

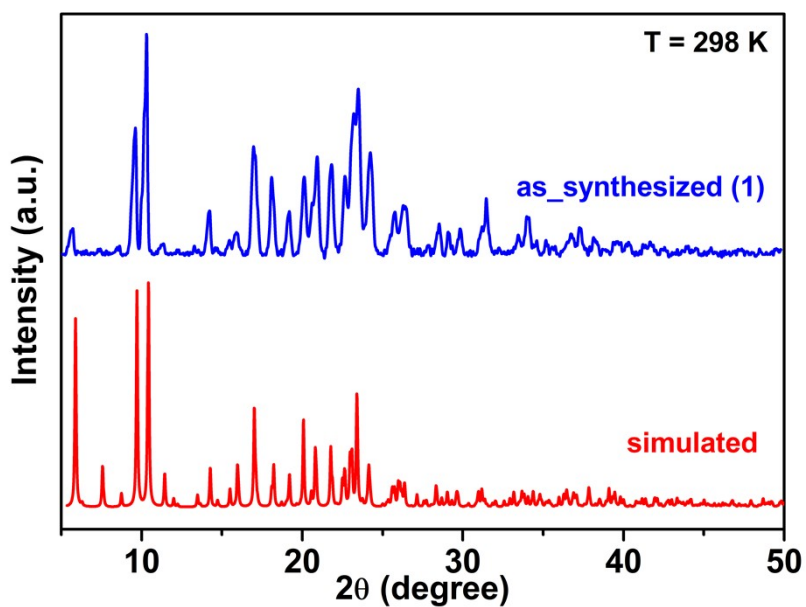
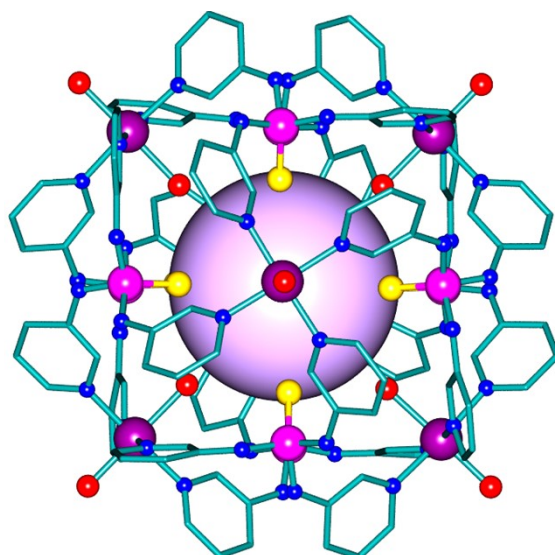
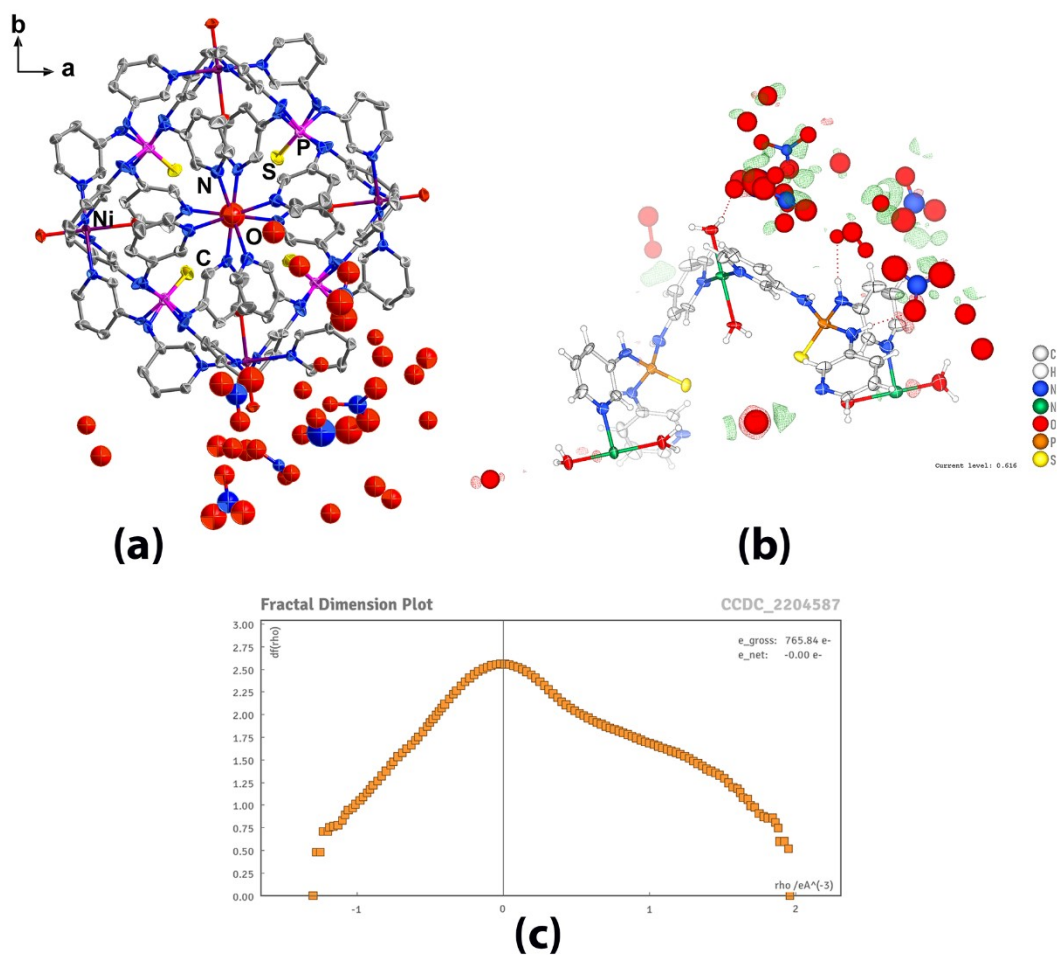


Figure S2 The powder X-ray diffraction profile of the as-synthesized compound 1 and its comparison with simulated pattern from single crystal X-ray data.



**Figure S3** Octahedral core structure of **1**, viewed along the four-fold axis.



**Figure S4** (a) Molecular structure of **1** viewed along the c-axis with 50% thermal ellipsoid probability. (b) Residual density map of the asymmetric unit of **1**. (c) Fractal dimension distribution of the residual density of **1** in the solvate region. We thank the crystallographic reviewer for providing the figures (b) and (c).

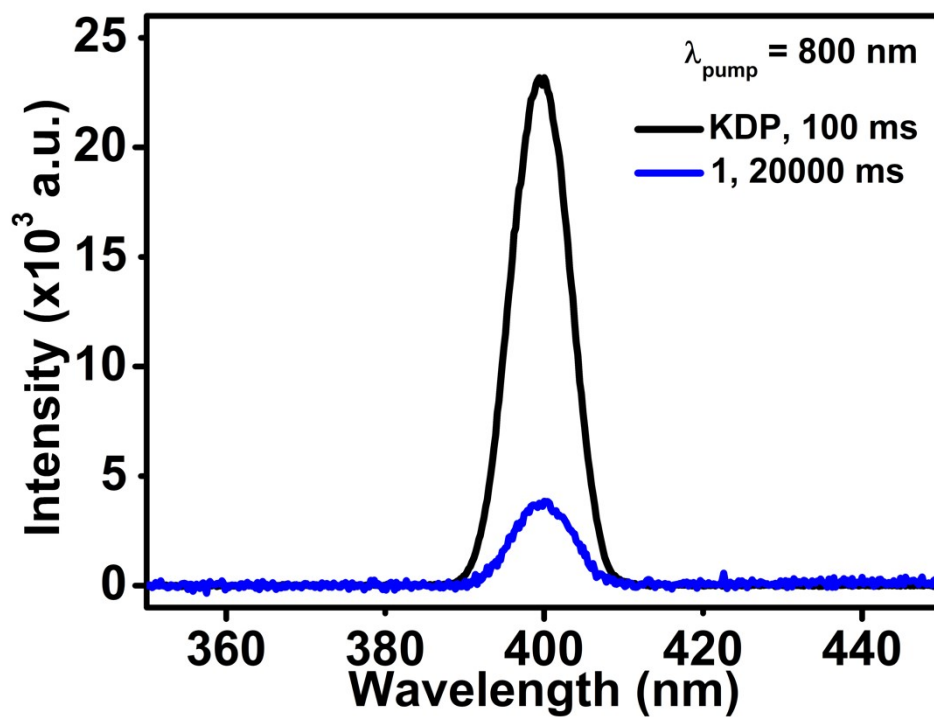


Figure S5 The SHG signal of **1** overlaid with that of KDP of the same particle size.

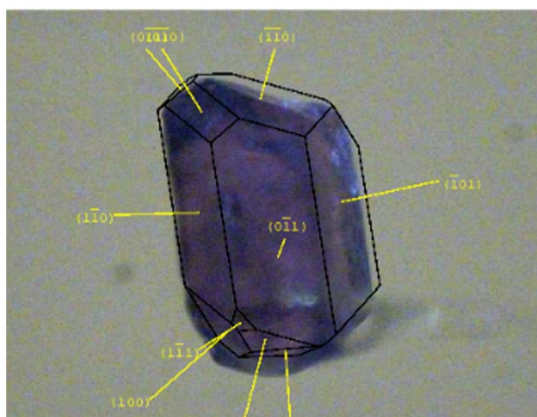


Figure S6 Face indexing pattern showing the various hkl planes on a single crystal of **1**.

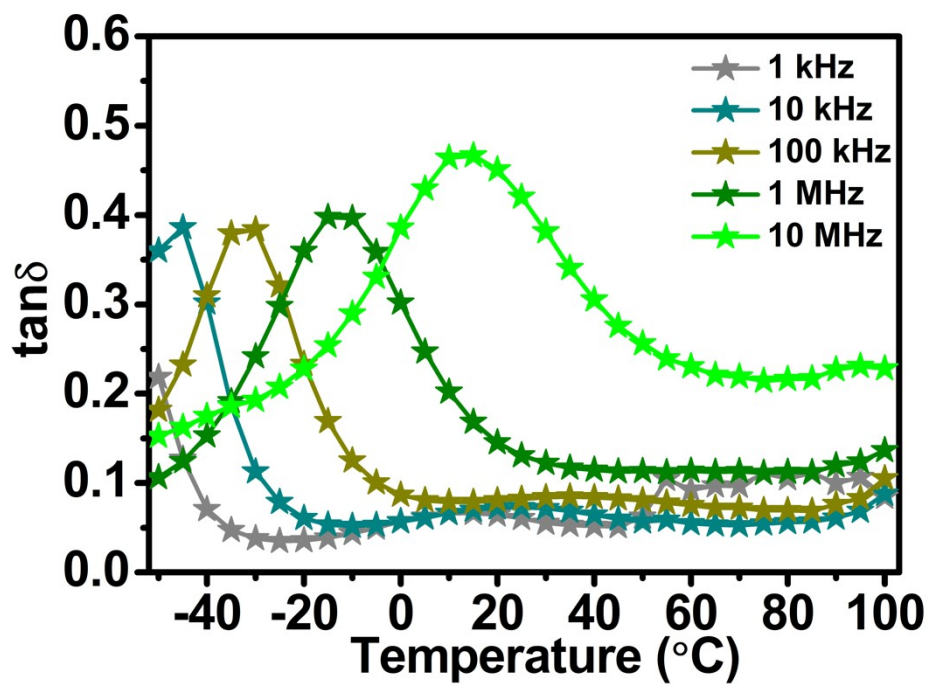


Figure S7 Dielectric loss factor ( $\tan \delta$ ) of 1 as a function of temperature.

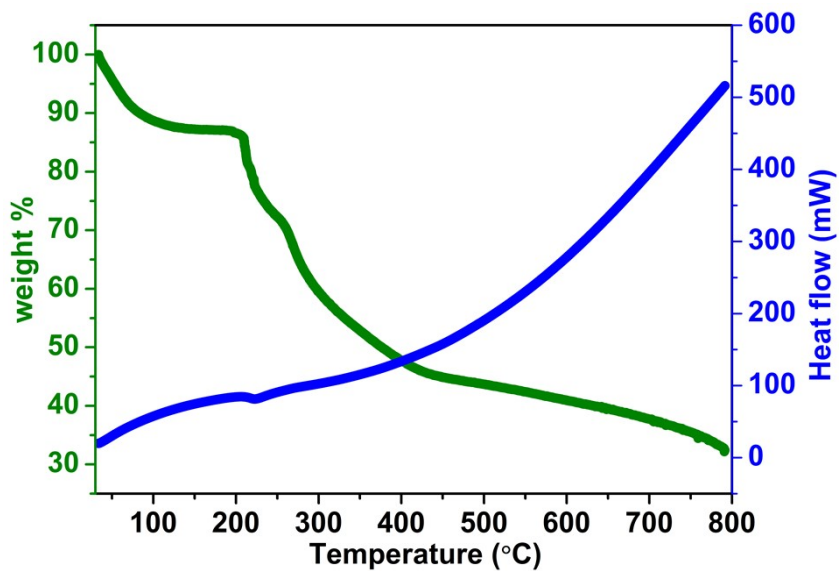


Figure S8 Thermo-gravimetric analysis (TGA) of 1.

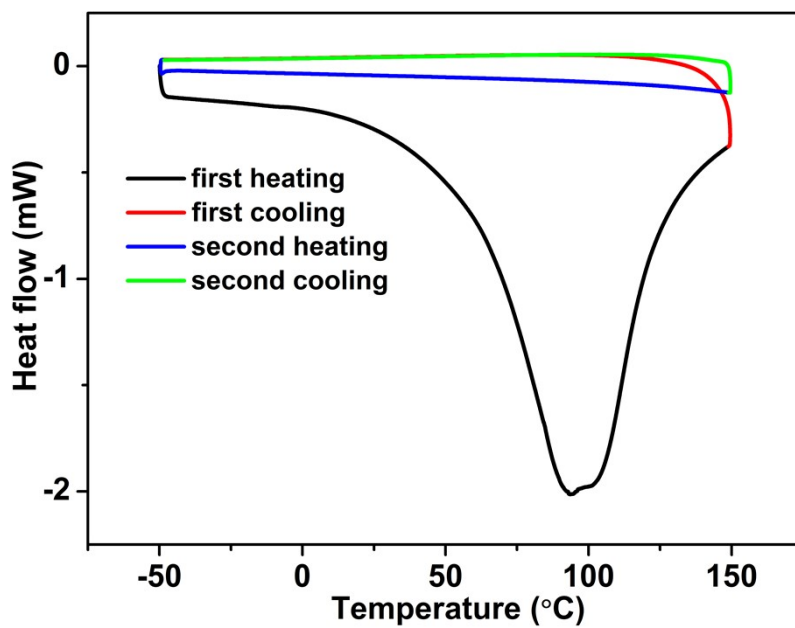


Figure S9 Differential Scanning Calorimetry (DSC) of 1.

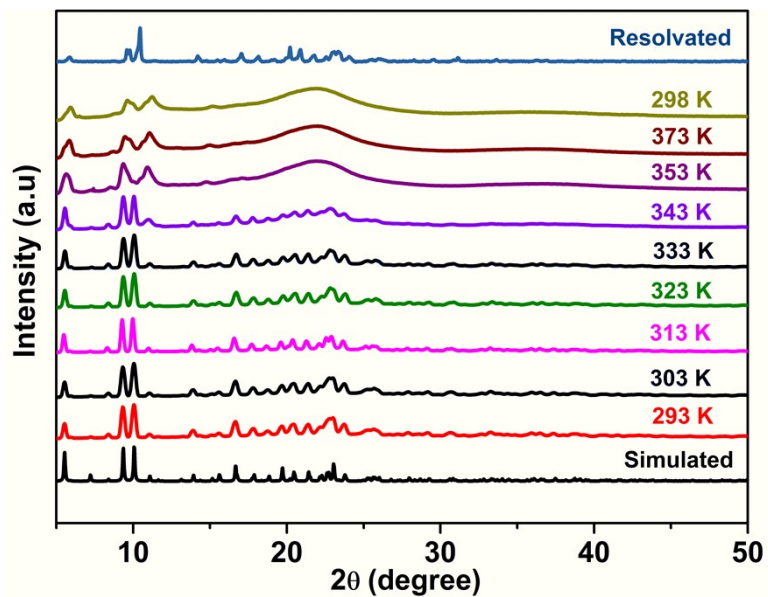


Figure S10 Variable-temperature PXRD of 1.

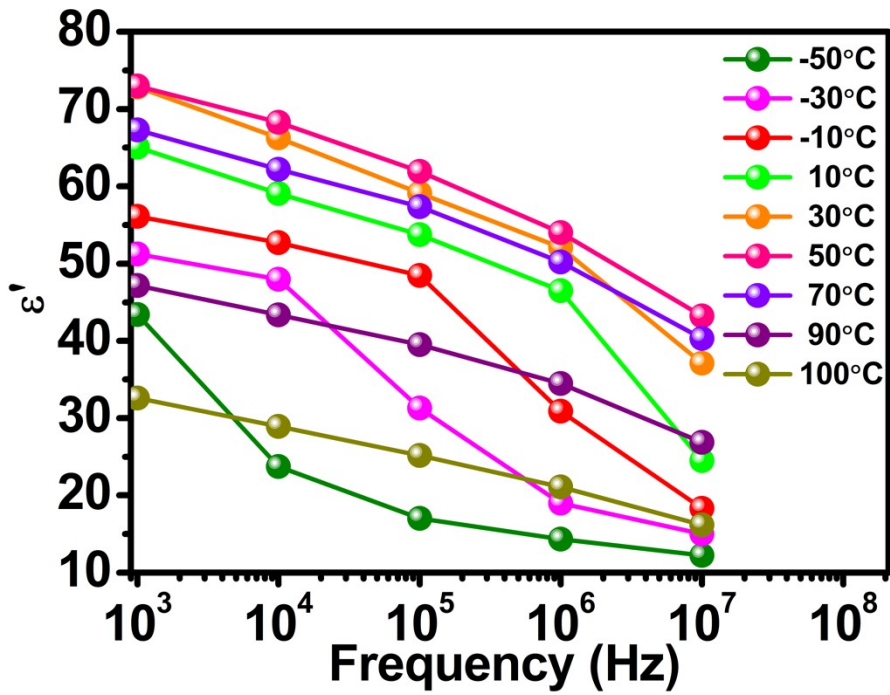


Figure S11 Real-part of the dielectric permittivity ( $\epsilon'$ ) graphs as a function of frequency.

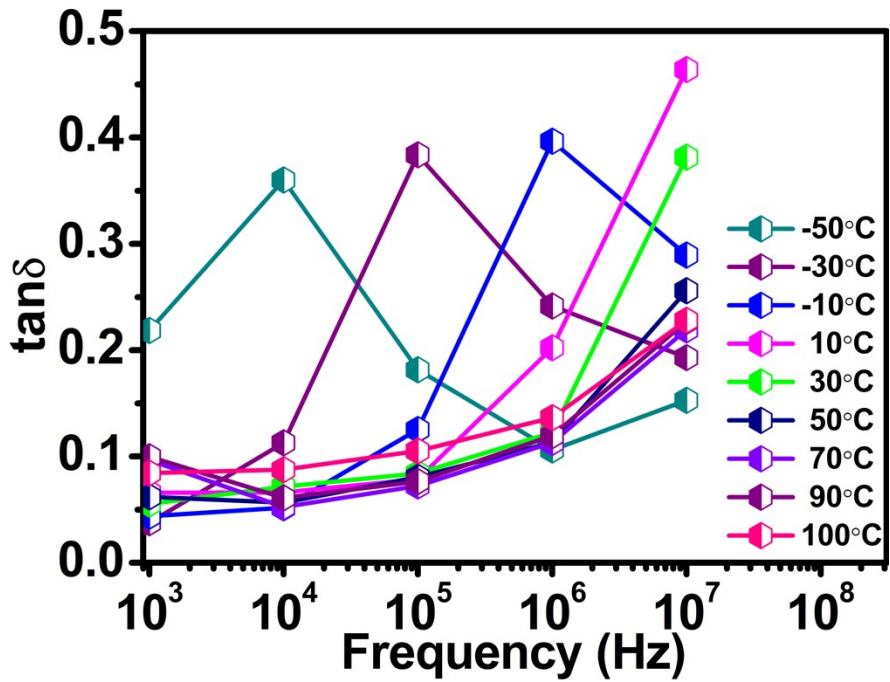
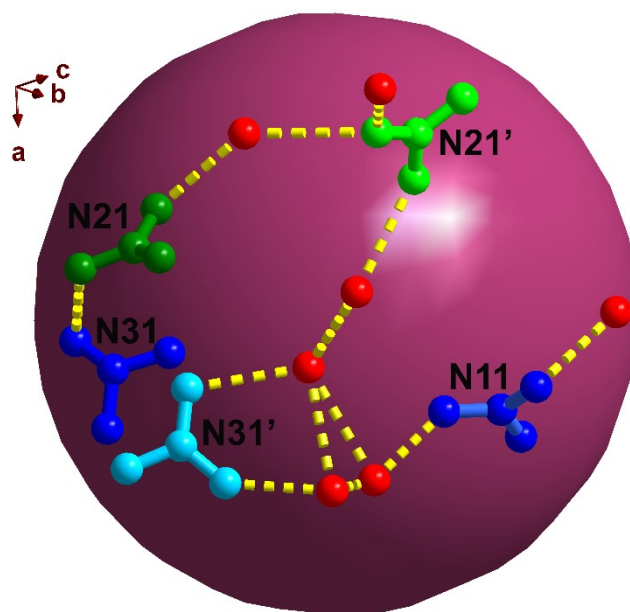
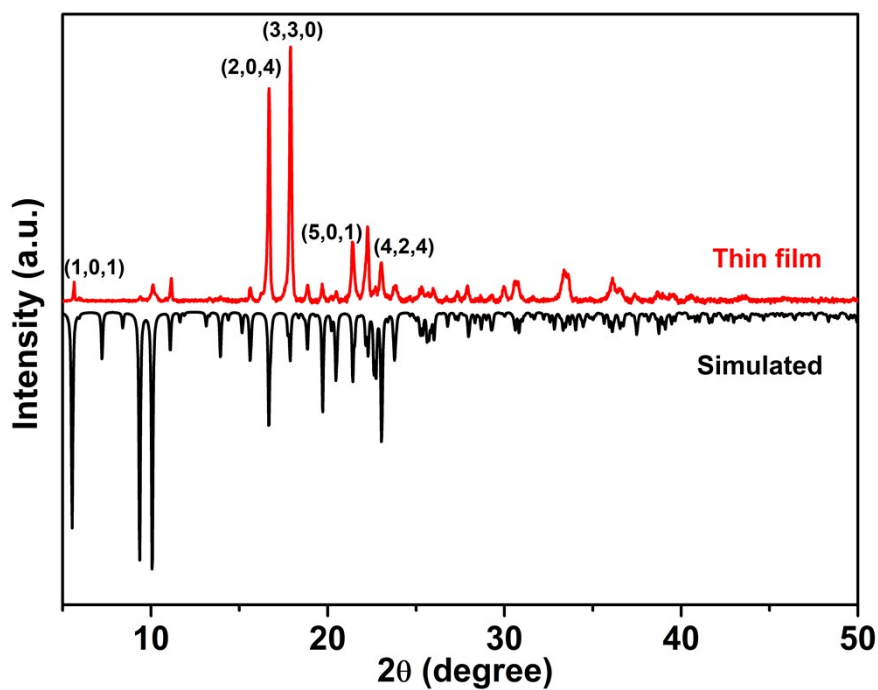


Figure S12 Dielectric loss factor ( $\tan \delta$ ) of 1 as a function of frequency.



**Figure S13** Segments of the ordered and the disordered nitrate anions and their H-bonding interactions with solvate molecules. The cyan and light green spheres indicate the disordered nitrate fragments.



**Figure S14** Powder X-ray diffraction pattern for the thin film of **1** and its comparison with simulated patterns from X-ray-derived structure.

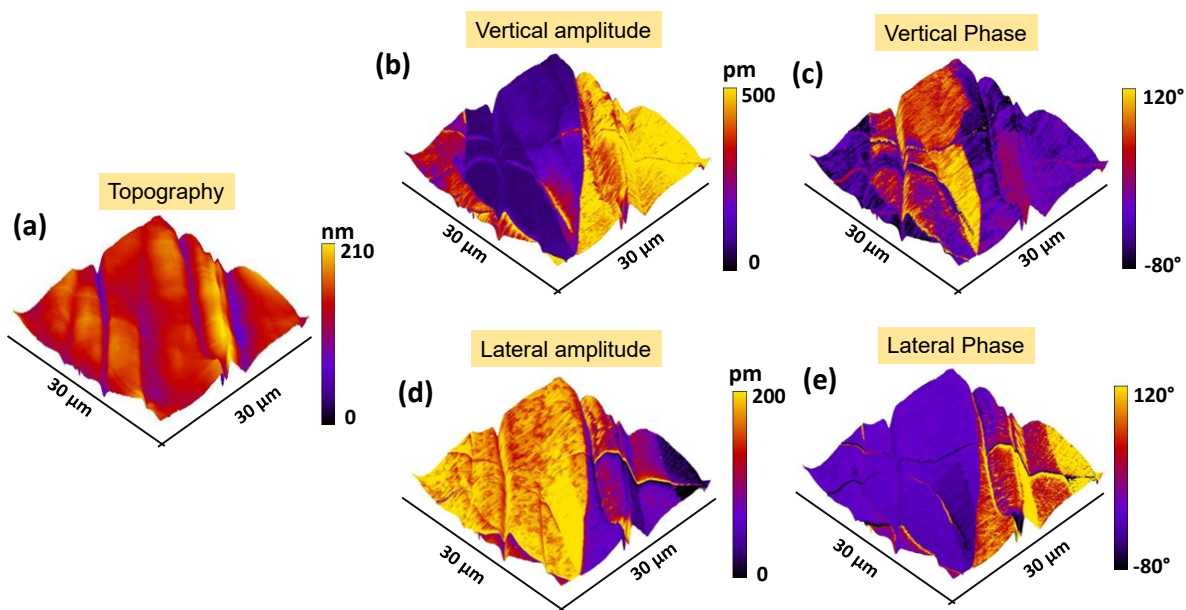


**Figure S15** Vertical and Lateral piezoresponse force microscopy (LPM) images on the thin film of **1** showing the (a) 3D topography (b) Vertical amplitude and (c) Vertical phase mappings overlaid on the 3D topography and (d) Lateral amplitude and (e) Lateral phase mappings overlaid on the 3D topography.

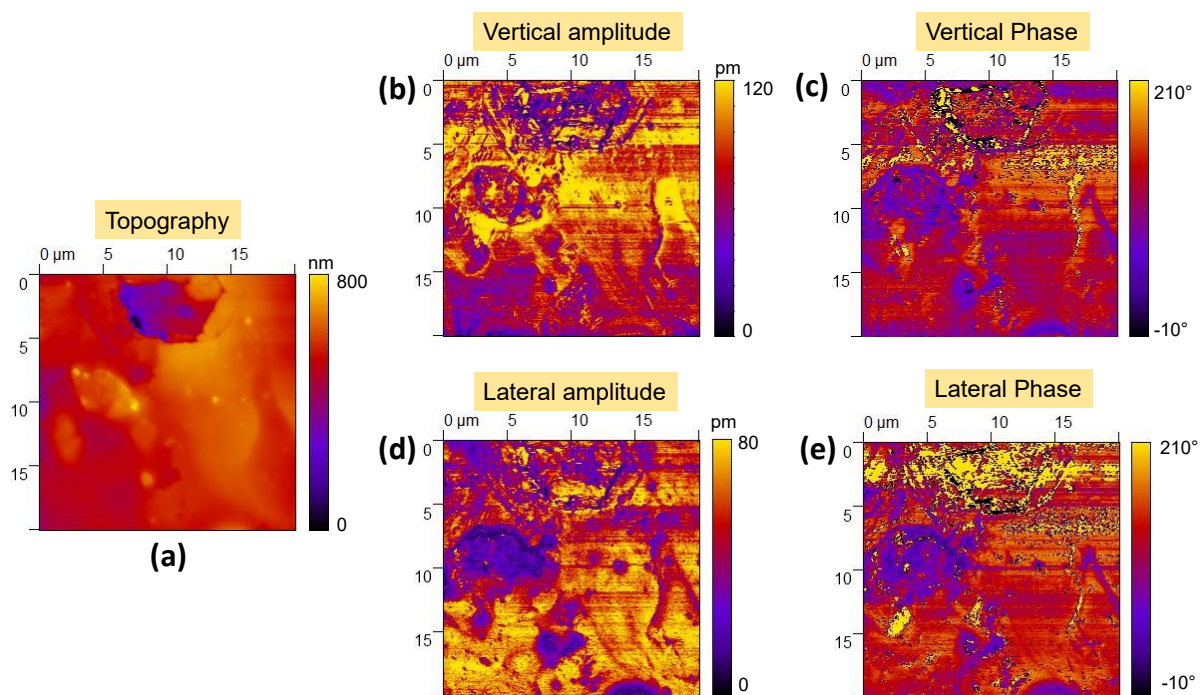


**Figure S16** PFM measurements on the bulk single crystal of **1**. (a) Topography (b) Vertical-Amplitude (c) Vertical-Phase (d) Lateral-Amplitude (e) Lateral-Phase images.

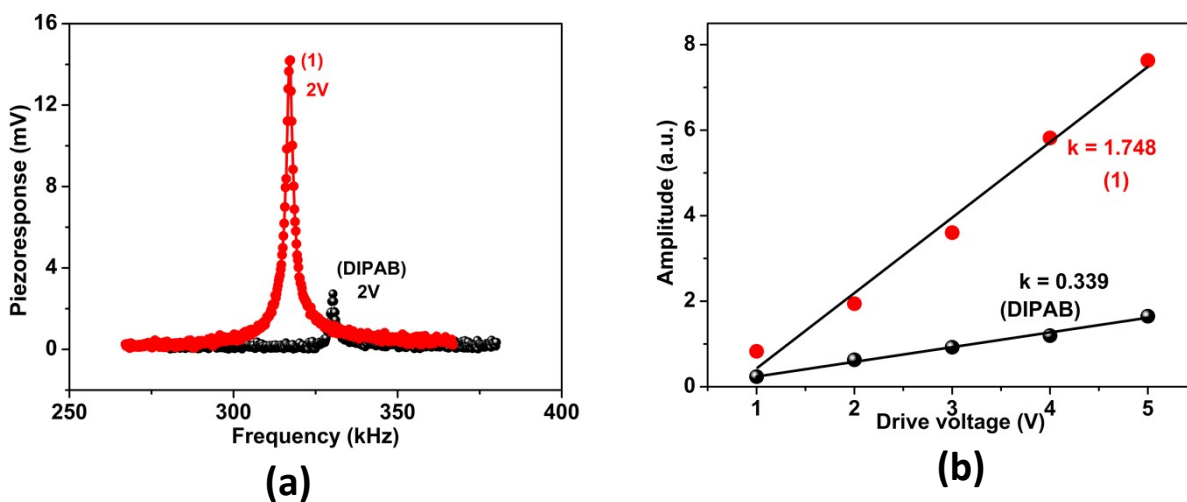


**Figure S17** Comparison of PFM (a) resonance peaks (b) effective piezoelectric coefficient of DIPAB (Diisopropyl ammonium bromide) and **1** (corrected by quality factor).

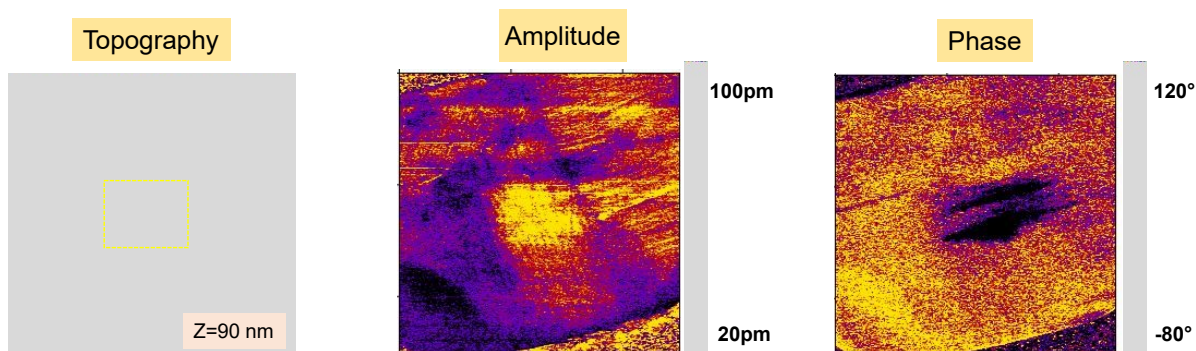


**Figure S18** PFM writing experiments on the thin film of **1**.

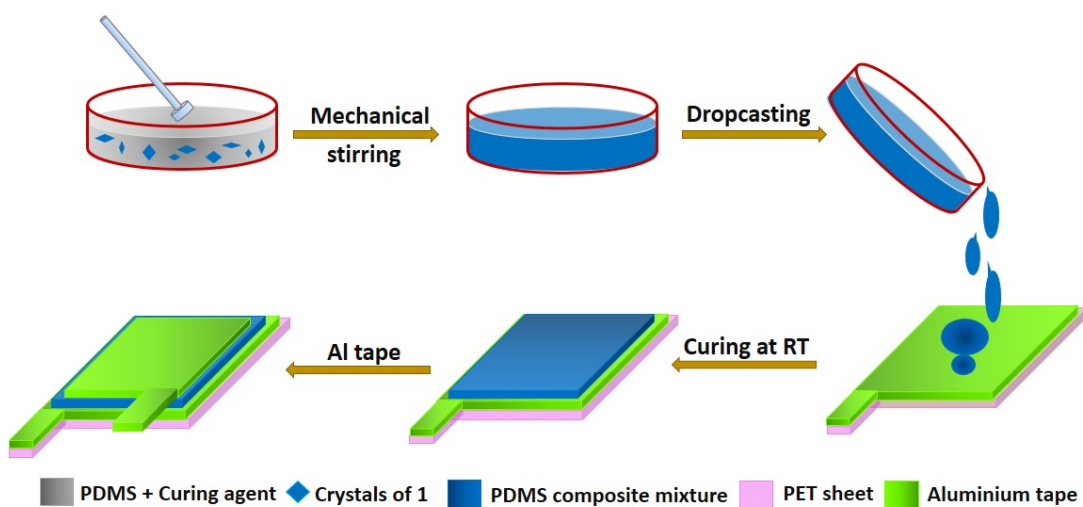


**Figure S19** Schematic diagram illustrating the preparation and fabrication of composite films of **1** in PDMS.

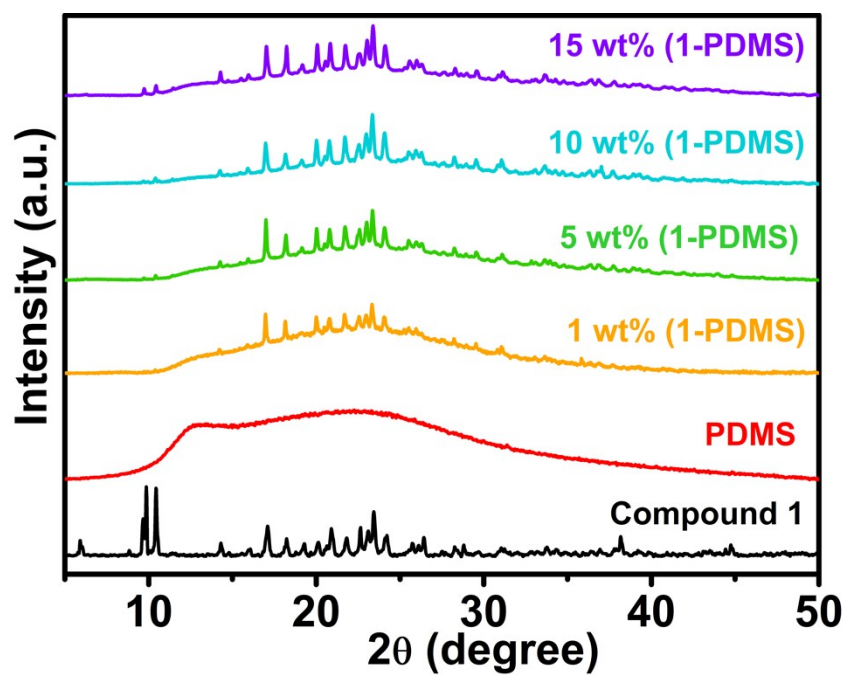


**Figure S20** PXRD profiles of various (1, 5, 10, 15) wt% 1-PDMS composite films and its comparison with pristine compound of **1**. The broad profile of a neat PDMS film shows its amorphous structure.

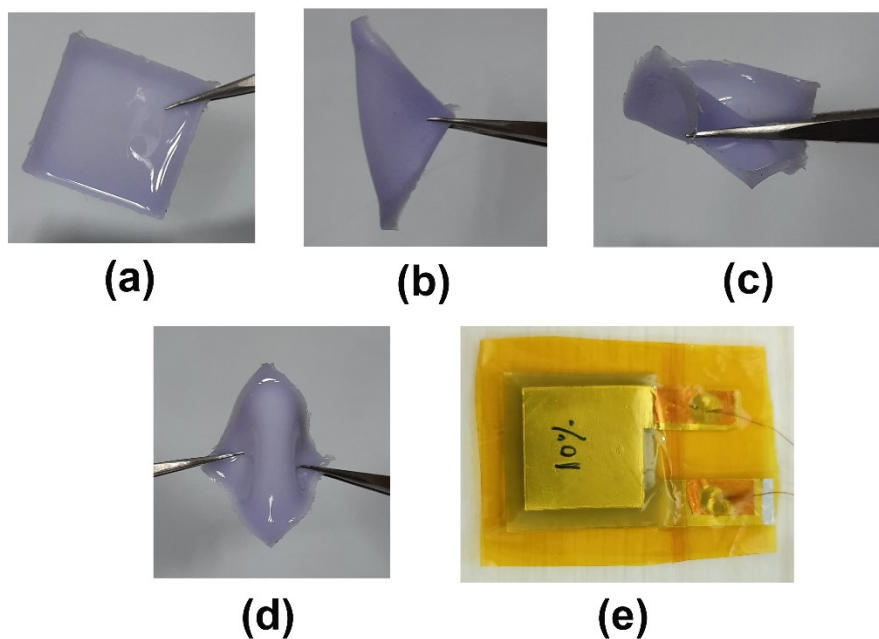


**Figure S21** Photographs of a representative (a) as-made composite film of **1**-PDMS showing its flexibility towards (b) folding, (c) two-fold bending and (d) twisting operations. (e) Photograph of a representative **1**-PDMS PENG device.

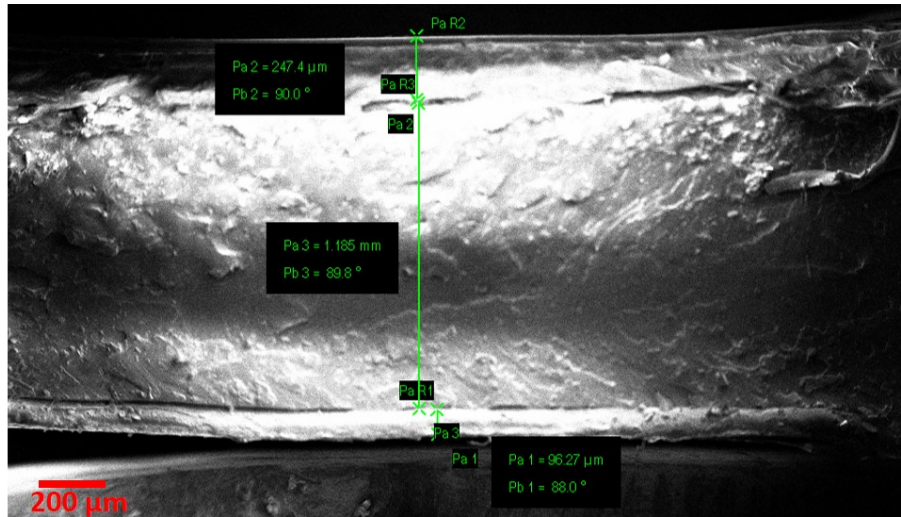


**Figure S22** The cross-sectional image of the sandwiched structure of a representative 1-PDMS composite film showing a thickness of around 1.19 mm.

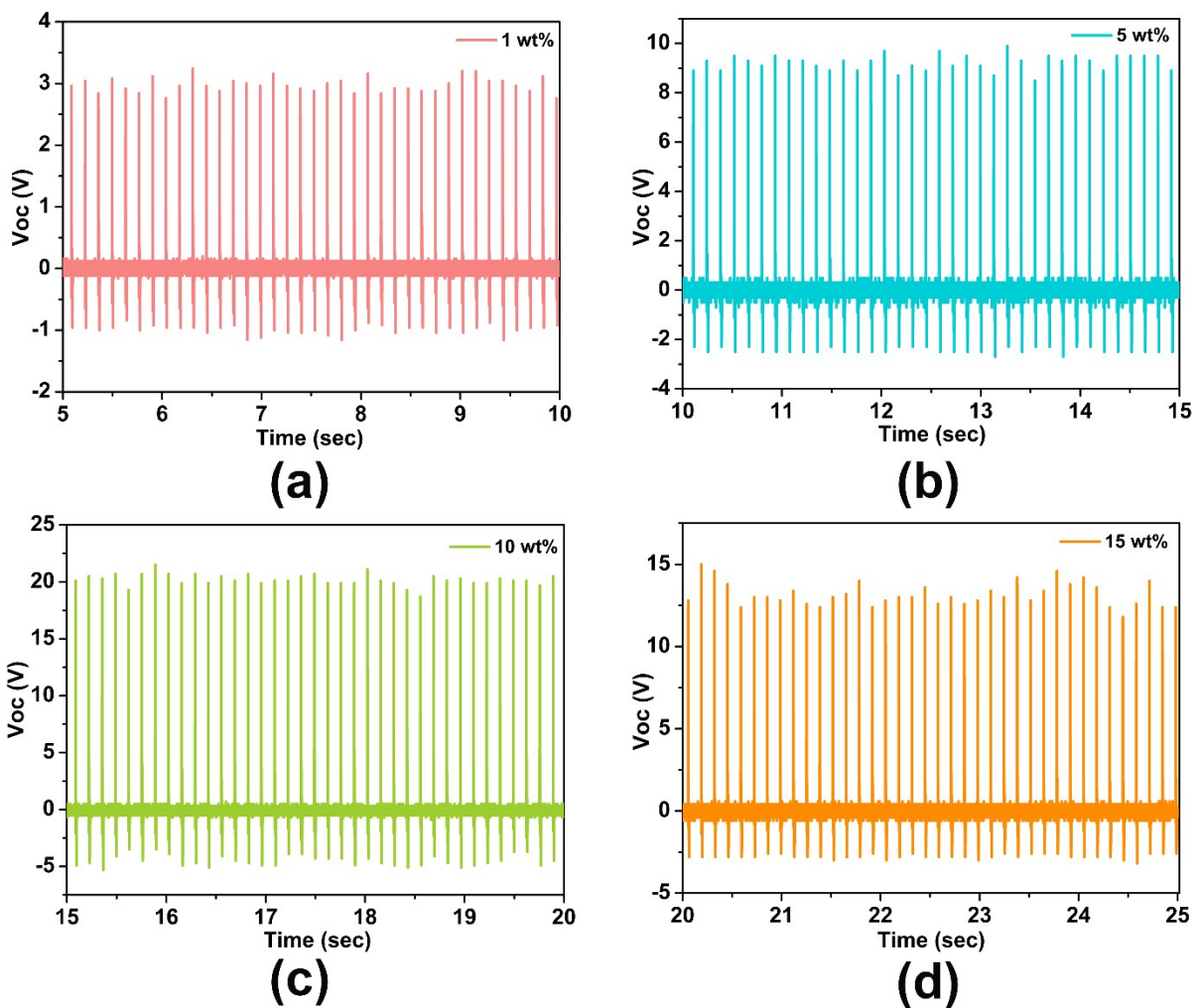


**Figure S23** The piezoelectric output open-circuit voltages of the various 1-PDMS PENG devices.

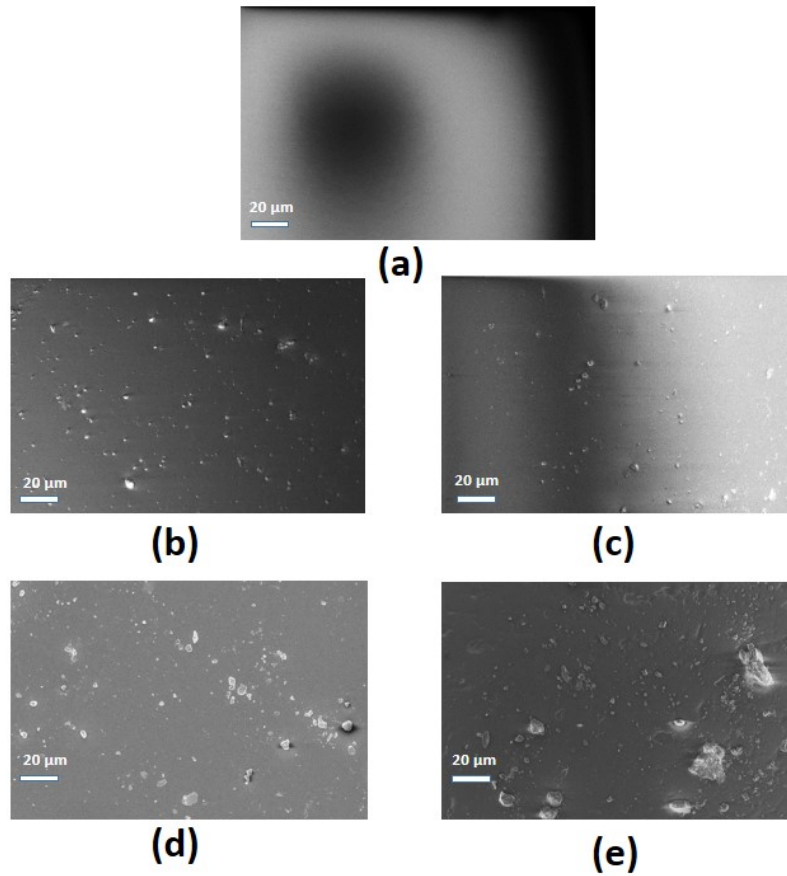


**Figure S24** SEM images of (a) neat PDMS film and the 1-PDMS composite films of (b) 1 wt% (c) 5 wt% (d) 10 wt% (e) 15 wt% of 1.

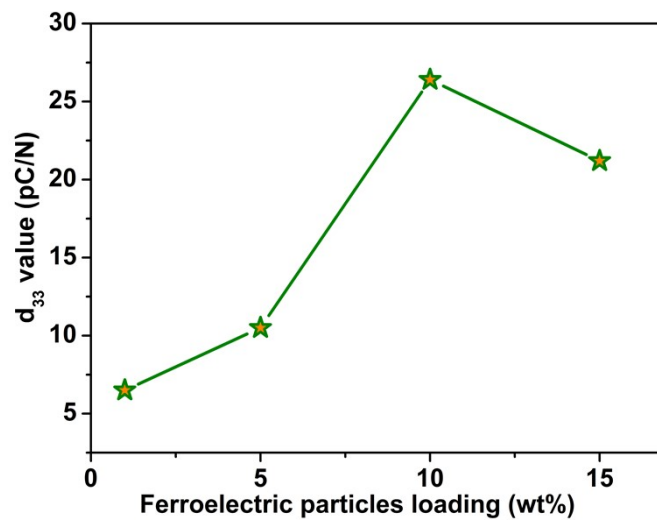


**Figure S25** The piezoelectric coefficient ( $d_{33}$ ) values obtained from the quasi-static method of the different weight percentage composite films.

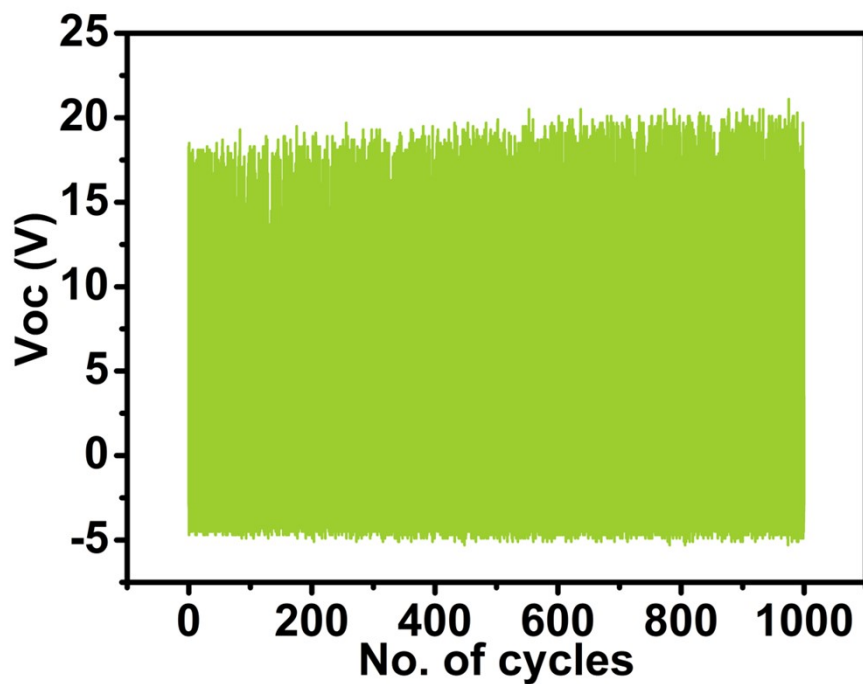


Figure S26 Long-term piezoelectric test performed for the 10 wt% 1-PDMS PENG device up to 1000 cycles.

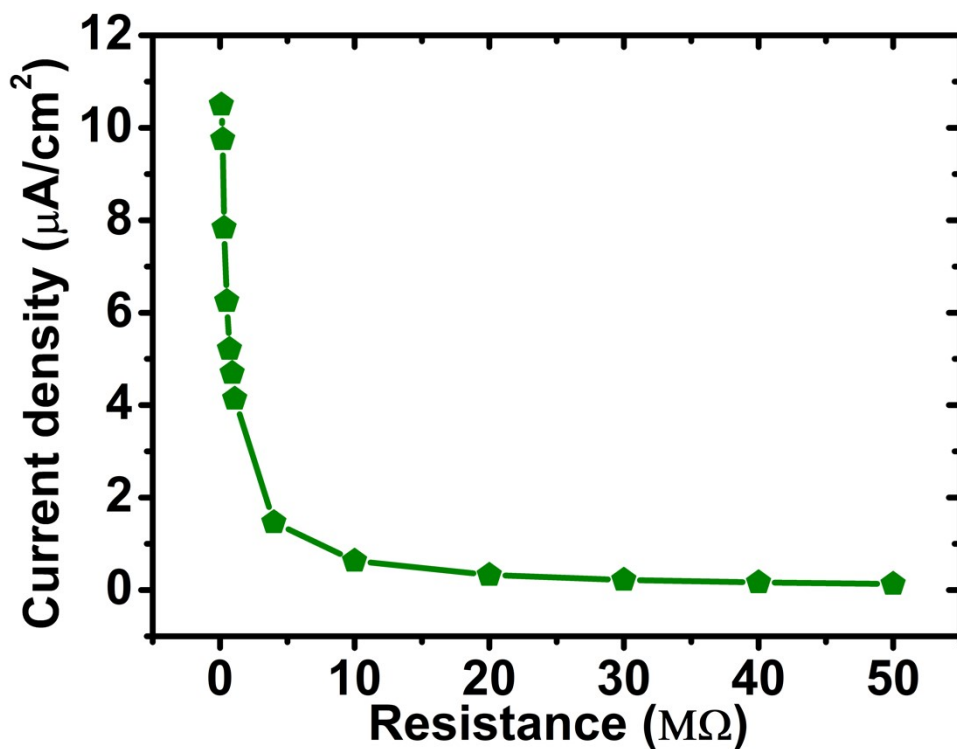


Figure S27 Calculated current density plot of 10 wt% 1-PDMS device across various load resistances.

**Table S2:** Comparison of output device performance of various piezoelectric energy harvesters based on metal-organic materials.

| Hybrid composite materials   | Output voltage (V) | Current/Current density       | Power/Power density            | Active Area                 | References       |
|--|--------------------|-------------------------------|--------------------------------|-----------------------------|------------------|
| Car_Zn (MeCN)-PDMS   | 2.5 V              | -                             | -                              | 1 x 1 cm <sup>2</sup>       | <b>6</b>         |
| Zr-MOF- PDMS   | 536 mV             | -                             | -                              | 2 x 1.5 cm <sup>2</sup>     | <b>7</b>         |
| [Ph <sub>3</sub> MeP] <sub>4</sub> [Ni(NCS) <sub>6</sub> ]-TPU                           | 19.29 V            | 3.59 μA/cm <sup>3</sup>       | 50.26 μW/cm <sup>3</sup>       | 1.3 x 3 cm <sup>2</sup>     | <b>8</b>         |
| (CdI <sub>2</sub> -INH=CMe <sub>2</sub> )-PVDF   | 12 V               | -                             | 32 μW/cm <sup>2</sup>          | 2 x 1 cm <sup>2</sup>       | <b>9</b>         |
| MAPI-PVDF  | 220 mV             | -                             | -                              | 2.9 x 1.5 cm <sup>2</sup>   | <b>10</b>        |
| (CdI <sub>2</sub> -NAP)-PVDF   | 22 V               | -                             | 24 μW/cm <sup>2</sup>          | 4 x 1.5 cm <sup>2</sup>     | <b>11</b>        |
| PVDF-PLLA-SnO <sub>2</sub> NF-MAPbI <sub>3</sub>   | 4.82 V             | 29.7 nA                       | -                              | 0.25 X 0.25 cm <sup>2</sup> | <b>12</b>        |
| (TMFM)FeBr <sub>4</sub>  | 2.2 V              | -                             | -                              | -                           | <b>5</b>         |
| MASnI <sub>3</sub> -PVDF   | 12 V               | 4 μA/cm <sup>2</sup>          | 21.6 μW/cm <sup>2</sup>        | -                           | <b>13</b>        |
| 5 wt% ([Zn(L <sup>1</sup> )(bpy)]·(H <sub>2</sub> O) <sub>1.5</sub> ) <sub>∞</sub> -TPU) | 5.6 V              | 6.19 μA/cm <sup>2</sup>       | 14.6 μW/cm <sup>2</sup>        | 1.3 x 2 cm <sup>2</sup>     | <b>14</b>        |
| <b>10 wt% (1-PDMS)</b>   | <b>25.35 V</b>     | <b>4.69 μA/cm<sup>2</sup></b> | <b>79.33 μW/cm<sup>2</sup></b> | <b>2 x 2 cm<sup>2</sup></b> | <b>This work</b> |

\*The overall performance of the composite devices depends on several factors, such as the dimensions of the composite films (including area, thickness), amount of piezoelectric fillers in polymer, active particles surface morphology, supporting polymer, electrodes, active surface area between electrode and composite film, magnitude of impact force and frequency.

Note – PDMS = Polydimethylsiloxane; PVDF = Polyvinyl difluoride; MAPI = Methylammonium Lead Iodide; PLLA = poly(L-lactic acid); (TMFM)FeBr<sub>4</sub> = trimethylfluoromethylammonium iron(III)bromide; MASnI<sub>3</sub> = methylammonium tin iodide.

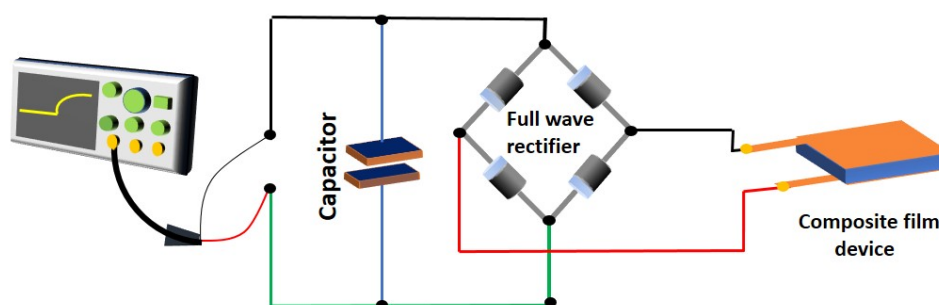


**Figure S28** Schematic drawing depicting the capacitor charging experiment using a 1-PDMS device connected through a full-wave bridge rectifier.

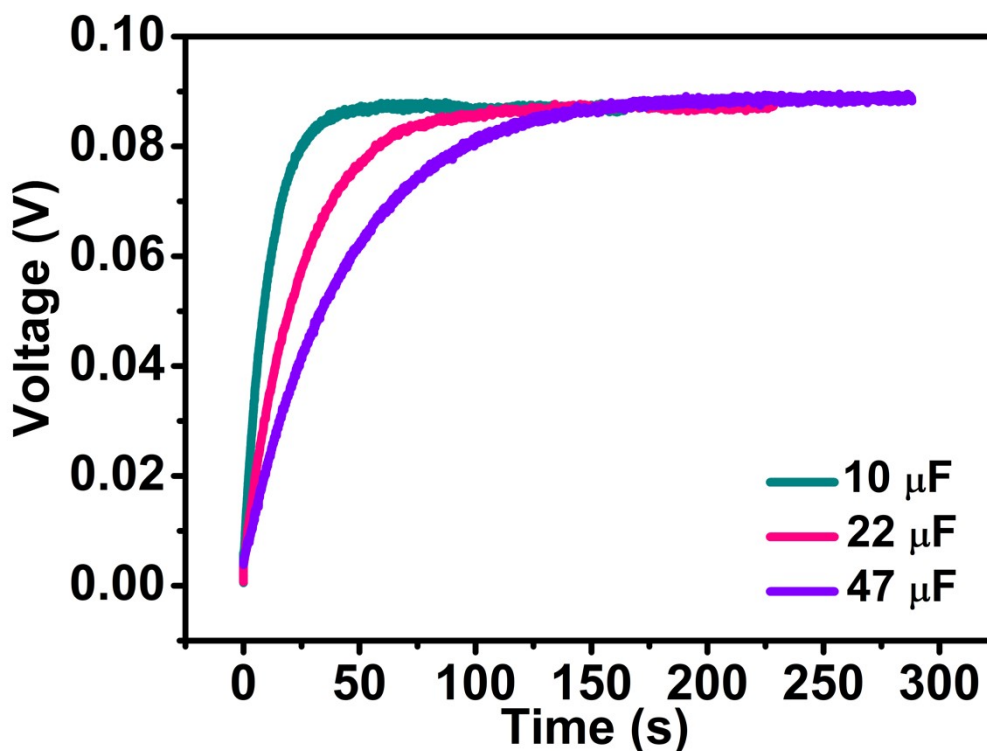


**Figure S29** The rectified-voltage signals for the different-rated capacitors in the charging experiment obtained by the continuous impact of the 10 wt% 1-PDMS device.

#### References

1. A. Yadav, A. K. Srivastava, P. Kulkarni, P. Divya, A. Steiner, B. Praveenkumar and R. Boomishankar, *J. Mater. Chem. C*, 2017, **5**, 10624-10629.
2. Y. Zhang, X.-J. Song, Z.-X. Zhang, D.-W. Fu and R.-G. Xiong, *Matter*, 2020, **2**, 697-710.
3. Meindl, K.; Henn, J.: Foundations of residual-density analysis. *Acta Crystallogr. A: Foundations of Crystallography* **2008**, *64*, 404-418.
4. S. K. Kurtz and T. T. Perry, *J. Appl. Phys.*, 1968, **39**, 3798-3813.
5. Y. Zhang, X.-J. Song, Z.-X. Zhang, D.-W. Fu and R.-G. Xiong, *Matter*, 2020, **2**, 697-710.
6. Y. Chen, S. Guerin, H. Yuan, J. O'Donnell, B. Xue, P.-A. Cazade, E. U. Haq, L. J. W. Shimon, S. Rencus-Lazar, S. A. M. Tofail, Y. Cao, D. Thompson, R. Yang and E. Gazit, *J. Am. Chem. Soc.*, 2022, **144**, 3468-3476.
7. B. H. Moghadam, M. Hasanzadeh and A. Simchi, *ACS Appl. Nano Mater.*, 2020, **3**, 8742-8752.
8. T. Vijayakanth, F. Ram, B. Praveenkumar, K. Shanmuganathan and R. Boomishankar, *Angew. Chem., Int. Ed.*, 2020, **59**, 10368-10373.
9. K. Roy, S. Jana, S. K. Ghosh, B. Mahanty, Z. Mallick, S. Sarkar, C. Sinha and D. Mandal, *Langmuir*, 2020, **36**, 11477-11489.

10. A. Sultana, S. K. Ghosh, M. M. Alam, P. Sadhukhan, K. Roy, M. Xie, C. R. Bowen, S. Sarkar, S. Das, T. R. Middy and D. Mandal, *ACS Appl. Mater. Interfaces*, 2019, **11**, 27279-27287.
11. K. Roy, S. Jana, Z. Mallick, S. K. Ghosh, B. Dutta, S. Sarkar, C. Sinha and D. Mandal, *Langmuir*, 2021, **37**, 7107-7117.
12. R. Tusiime, F. Zabihi, M. Tebyetekerwa, Y. M. Yousry, Y. Wu, M. Eslamian, S. Yang, S. Ramakrishna, M. Yu and H. Zhang, *J. Mater. Chem. C*, 2020, **8**, 2643-2658.
13. S. Ippili, V. Jella, J.-H. Eom, J. Kim, S. Hong, J.-S. Choi, V.-D. Tran, N. Van Hieu, Y.-J. Kim, H.-J. Kim and S.-G. Yoon, *Nano Energy*, 2019, **57**, 911-923.
14. N. Prajesh, V. B. Sharma, S. S. Rajput, C. K. Singh, P. Dixit, B. Praveenkumar, J. K. Zaręba, D. Kabra, S. Ogale and R. Boomishankar, *ACS Sustainable Chem. Eng.*, 2022, **10**, 9911-9920.